

A simplified method to estimate tidal current effects on the ocean wave power resource

Hashemi, M. Reza ; Grilli, Stephan T.; Neill, Simon

Renewable Energy

DOI:

[10.1016/j.renene.2016.04.073](https://doi.org/10.1016/j.renene.2016.04.073)

Published: 01/10/2016

Peer reviewed version

[Cyswllt i'r cyhoeddiad / Link to publication](#)

Dyfyniad o'r fersiwn a gyhoeddwyd / Citation for published version (APA):

Hashemi, M. R., Grilli, S. T., & Neill, S. (2016). A simplified method to estimate tidal current effects on the ocean wave power resource. *Renewable Energy*, 96(Part A), 257-269.
<https://doi.org/10.1016/j.renene.2016.04.073>

Hawliau Cyffredinol / General rights

Copyright and moral rights for the publications made accessible in the public portal are retained by the authors and/or other copyright owners and it is a condition of accessing publications that users recognise and abide by the legal requirements associated with these rights.

- Users may download and print one copy of any publication from the public portal for the purpose of private study or research.
- You may not further distribute the material or use it for any profit-making activity or commercial gain
- You may freely distribute the URL identifying the publication in the public portal ?

Take down policy

If you believe that this document breaches copyright please contact us providing details, and we will remove access to the work immediately and investigate your claim.

1 A simplified method to estimate tidal current effects on
2 the ocean wave power resource

3 M. Reza Hashemi,^{a,1}, Stéphan T. Grilli^a, Simon P. Neill^b

4 ^a*Department of Ocean Engineering and Graduate School of Oceanography, University of*
5 *Rhode Island, USA*

6 ^b*School of Ocean Sciences, Bangor University, Menai Bridge, UK*

7 **Abstract**

8 Although ocean wave power can be significantly modified by tidal currents,
9 resource assessments at wave energy sites generally ignore this effect, mainly
10 due to the difficulties and high computational cost of developing coupled
11 wave-tide models. Furthermore, validating the prediction of wave-current in-
12 teraction effects in a coupled model is a challenging task, due to the paucity
13 of observational data. Here, as an alternative to fully coupled numerical
14 models, we present a simplified analytical method, based on linear wave the-
15 ory, to estimate the influence of tidal currents on the wave power resource.
16 The method estimates the resulting increase (or decrease) in wave height and
17 wavelength for opposing (or following) currents, as well as quantifying the
18 change in wave power. The method is validated by applying it to two en-
19 ergetic locations around the UK shelf - Pentland Firth and Bristol Channel
20 - where wave/current interactions are significant, and for which field data
21 are available. Results demonstrate a good accuracy of the simplified an-
22 alytical approach, which can thus be used as an efficient tool for making
23 rapid estimates of tidal effects on the wave power resource. Additionally, the
24 method can be used to help better interpret numerical model results, as well

¹Corresponding author,
Email: reza.hashemi@uri.edu

25 as observational data.

26 *Keywords:* Wave-current interactions, Resource assessment, Wave power,
27 Pentland Firth, Bristol Channel

28 **1. Introduction**

29 The exploitation of ocean wave power as a renewable energy resource has
30 generated much interest in academia and industry, and has inspired many
31 inventors, with more than one thousand patents registered to date for wave
32 energy technologies [1]. The accurate assessment of site-specific ocean wave
33 resource is the first step in developing projects for wave energy extraction
34 [2].

35 Wave-current interactions are routinely ignored in such resource assess-
36 ments (e.g. [3, 4]), despite earlier research that illustrates the significant
37 influence of tidal currents on wave properties, such as height and wavelength
38 [5, 6, 7]. This is partly due to the high computational cost associated with
39 running coupled wave-tide models; also, validating wave-current iteration ef-
40 fects in numerical models is a challenging task due the paucity of observations
41 and the complexity of the physical processes involved.

42 The effect of tidal currents on the wave power resource has been con-
43 sidered in a few studies to date, on the basis of coupled wave-tide models.
44 Barbariol et al. [8] demonstrated that the inclusion of wave-current interac-
45 tion (WCI) effects could yield up to a 30% difference in wave power estimates
46 at a location off the Gulf of Venice. The ROMS (Regional Ocean Modelling
47 System) ocean model and SWAN (Simulating WAVE Nearshore) wave model
48 were used in coupled mode to conduct this study. Using the same mod-

49 elling approach, Hashemi and Neill [9] showed that tidal currents can alter
 50 wave power by more than 10% in some regions of the northwest European
 51 shelf seas. They also briefly discussed a simple method to calculate this ef-
 52 fect. However, in their method, they only considered the effect of tides on
 53 the wave group velocity, but on wave height, which might be greater, was
 54 ignored. Furthermore, due to this limitation, no comparison with observa-
 55 tions was made - which could have assessed the accuracy of the method.
 56 Saruwatari et al. [10] used a coupled model (SWAN and MOHID Water
 57 Modelling System [11]) to study the effect of the WCI on the wave power,
 58 around the Orkney. They reported an up to 200% increase in wave height,
 59 when waves and currents are opposite. However, they did not demonstrate
 60 that their coupled model improved the wave simulation, in comparison to a
 61 decoupled SWAN model.

62 In this research, a simplified but adequately accurate and efficient analyt-
 63 ical method is proposed to estimate the effect of tidal currents on the wave
 64 power resource. Wave power, in general, is proportional to the wave group
 65 velocity and the wave height squared (see Eq. 1); hence, WCI effects on both
 66 properties are included in the method. A limitation is that the method as-
 67 sumes waves are either following or opposing the currents. This assumption
 68 is valid in the majority of laboratory studies [12] and also applies in the field
 69 to many wave energy sites [13].

2. Methods

2.1. Theoretical background

Both wave height - which quantifies the magnitude of wave energy - and group velocity - which is the speed of wave energy transport - are modified by tidal currents. Here, we present a simple analytical method, based on linear wave theory, for estimating these changes as a function of the current velocity, when currents and waves are aligned (opposing or following). We will only consider deep water waves (or nearly), for which linear theory is a reasonable approximation. We will also assume that the current field is specified (i.e., the effect of waves on currents is neglected).

2.1.1. Wave power in the absence of tides

In water of depth h and in the absence of a current, the period-averaged energy flux per unit width of wave crest (i.e. the mean wave power P_o in W/m) is equal to the mean rate of work done by the dynamic pressure over a wave period². According to linear wave theory, for a monochromatic wave of period T_o and height H_o , this is given by [14],

$$P_o = E_{fo} = E_o C_{go} = \left\{ \frac{1}{8} \rho g H_o^2 \right\} C_{go}; \quad C_{go} = \frac{\sigma_o}{k_o} \left\{ \frac{1}{2} \left(1 + \frac{2k_o h}{\sinh 2k_o h} \right) \right\} \quad (1)$$

where C_{go} is the group velocity, E_o is mean wave energy, $\sigma_o = 2\pi/T_o$ is the wave angular frequency, and $k_o = 2\pi/L_o$ is the wave number (with L_o the wave length). The subscript o indicates that wave properties are evaluated *in*

² $\frac{1}{T} \int_0^T \int_{-h}^{\eta} p_D u_w dz dt$, where p_D is the dynamic pressure and u_w is the horizontal wave induced particle velocity, and η the wave surface elevation.

the absence of a background current. The angular frequency and wavenumber are related to water depth by the linear dispersion relationship,

$$\sigma_0^2 = gk_o \tanh(k_o h) \quad (2)$$

For deep water waves, i.e., $k_o h \geq \pi$ [14], $\tanh(k_o h) \simeq 1$ in Eq. (2) and $k_o \simeq \sigma_o^2/g$. Hence, in Eq. (1), we have $C_{go} \simeq g/(2\sigma_o) = gT_o/(4\pi)$, which leads to,

$$P_o = \frac{\rho g}{32\pi} H_o^2 T_o \quad (3)$$

For irregular waves described by a wave energy spectrum, with significant wave height H_{so} and wave energy period T_{eo} , H_o would be replaced in Eq. (3) by the root-mean-square (RMS) wave height $H_{o,RMS}$ (with, in deep water, $H_{o,RMS} = H_{so}/\sqrt{2}$) and T_o by an equivalent “energy” wave period T_{eo} (see Table 1 for the definition of the energy period based on a wave energy spectrum).

2.1.2. Wave power in the presence of tidal currents

When a monochromatic wave propagates in the presence of a tidal current of magnitude u (projected in the direction of wave propagation), the wave energy flux is no longer conserved, due to energy exchange between the wave and current fields. Instead, the total period-averaged energy flux (or transport) E_{tf} is conserved, which in a vertical plane comprises other terms

105 such as the kinetic energy of the current³, and is given by (e.g. [15, 16]),

$$E_{tf} = \underbrace{[E C_g]}_{(i)} + \underbrace{[E u]}_{(ii)} + \underbrace{\left[\frac{1}{2}\rho g h u^3\right]}_{(iii)} + \underbrace{\left[u \left(2\frac{C_g}{C} - \frac{1}{2}\right) E\right]}_{(iv)} = \text{cst} \quad (4)$$

106 where each term on the right-hand-side is interpreted as follows:

107 *i*: wave energy transport by the group velocity; relative wave power;

108 *ii*: wave energy transport by the projected tidal current;

109 *iii*: transport of the kinetic energy of tidal current;

110 *iv*: work done by the current against the wave radiation stress (i.e., energy
111 exchange between waves and currents; the radiation stress represents the
112 mean wave-induced excess momentum flux).

113 The total energy flux due to waves E_f (i.e., the absolute wave power) is
114 defined as the sum of the first and second terms in Eq. (4). Additionally,
115 due to the Doppler shift induced by the current [14], the angular frequency
116 of waves from the perspective of a stationary observer (i.e., the absolute
117 frequency σ_0) will be different from the intrinsic/relative wave frequency σ
118 (i.e., the wave frequency observed when moving with the current, for which
119 linear wave theory applies). We have,

$$\sigma_o = \sigma + k u \quad (5)$$

120 which as expected predicts a reduced/increased relative frequency for a co-
121 flowing/opposite current, respectively.

³ $E_{tf} = \frac{1}{T} \int_0^T \int_{-h}^{\eta} [p_D + \rho g \eta + \frac{1}{2} u \rho |\mathbf{u} + \mathbf{u}_w|^2] u_w dz dt.$

122 The presence of additional terms in Eq. (4) introduces some difficulties in
 123 the direct application of the energy flux conservation law. For this reason, in
 124 state-of-the-art phase-averaged wave models (e.g., SWAN [17]) one instead
 125 expresses the conservation of wave action E/σ [18, 19] which, unlike the total
 126 wave energy flux, is conserved in the presence of an ambient current. In a
 127 one-dimensional case, it reads,

$$\frac{\partial(E/\sigma)}{\partial t} + \frac{\partial \{[u(x, t) + C_g](E/\sigma)\}}{\partial t} = 0 \quad (6)$$

128 Besides wave energy - or wave height - the wave angular frequency and
 129 wavenumber are unknown in the above equation, which requires using addi-
 130 tional equations. Assuming linear wave theory, these are the linear disper-
 131 sion relationship Eq. (2) and the conservation of wave crests equation (i.e.
 132 $\frac{\partial k}{\partial t} + \frac{\partial \sigma_o}{\partial x} = 0$; [20, 14]), which together with Eq. (5) lead to the well-posed
 133 system of equations,

$$\left\{ \begin{array}{l} \frac{\partial k}{\partial t} + \frac{\partial \{\sigma + ku(x, t)\}}{\partial x} = 0 \\ \sigma^2 - gk \tanh(kh) = 0 \\ \frac{\partial (H^2/\sigma)}{\partial t} + \frac{\partial \{[u(x, t) + C_g(k, h, \sigma)]H^2/\sigma\}}{\partial x} = 0 \end{array} \right. \quad (7)$$

134 By replacing σ from the second into the first Eq. (7), each of the above
 135 equations can be independently solved for k , σ , and H , respectively.

136 Note that, using Eq. (5), the dispersion relationship for the relative

frequency (2nd Eq. (7)) can also be expressed as,

$$\sigma_o^2 \left\{ 1 - \frac{u}{C} \right\}^2 = gk \tanh(kh) \quad (8)$$

where $C = \sigma_o/k$ is the relative wave phase speed. Given σ_o , u and h , Eq. (8) can be solved numerically to find k .

2.2. The simplified method

Since the tidal period is much greater than the wave period, it is reasonable to assume a quasi-steady state, for which both the magnitude and direction of the tidal current can be considered as stationary with respect to the wave field, i.e., $\frac{\partial}{\partial t} \simeq 0$ in Eq. (7). Given the wave properties in the absence of a tidal current, H_o and σ_o in depth h , the modified properties when there is a tidal current u can be found based on Eqs. (7),

$$\text{1st} \rightarrow \sigma_o = \sqrt{gk \tanh(kh)} + ku(x) = \text{cst} \rightarrow \boxed{k = \checkmark}$$

$$\text{2nd} \rightarrow \sigma = \sigma_o - ku(x) \rightarrow \boxed{\sigma \ \& \ C_g = \checkmark}$$

$$\text{3rd} \rightarrow [C_{go}] \frac{H_o^2}{\sigma_o} = [u(x) + C_g] \frac{H^2}{\sigma} = \text{cst} \rightarrow \boxed{H/H_o = \checkmark}$$

Note that, as indicated before, k can also be found by solving Eq. (8), and the 2nd Eq. (1) is used to calculate C_{go} and C_g .

2.2.1. Deep water approximation for quasi-steady case

The three steps described above to find wave properties in the presence of a tidal current first require solving the transcendental equation for k , which can easily be implemented numerically. However, a closed form relationship

156 can be derived for this equation when assuming deep water waves, which as
 157 discussed before implies, $\sigma^2 \simeq gk$ (in 2nd Eq. (7) or Eq. (8)). Solving Eq.
 158 8, we find [14],

$$C = \frac{\sigma_o}{k} = u + \frac{C_o}{2} \left\{ 1 + \sqrt{1 + \frac{4u}{C_o}} \right\} \quad (9)$$

159 with $C_o = g/\sigma_o$, the wave phase speed. A deep water approximation is often
 160 valid for wind generated waves in the vicinity of wave energy devices. The
 161 range of water depths where wave energy converters are installed varies de-
 162 pending on the type of device; for instance, oscillatory devices are typically
 163 installed in more than a 40 m depth [2] and Pelamis is designed for a 50 m
 164 depth [21]. In practice, owing to the small slope of the tanh function near
 165 the deep water limit, the $kh \geq \pi$ requirement, which ensures a few percent
 166 errors on the linear dispersion relationship, can be somewhat extended into
 167 shallower waters. Thus, a relatively large wave with a period $T = 8$ s prop-
 168 agating in a $h = 40$ m water depth, has a $L = 2\pi/k = 96$ m wavelength, and
 169 thus $kh = 2.52 < \pi$; but for this wave, $\tanh(kh) = 0.96$, and the deep water
 170 approximation estimates the wavelength at 100 m, which is still reasonably
 171 accurate.

172 Based on Eq. (9) and the earlier equations simplified when assuming deep
 173 water waves, Table 2 summarizes the various closed form relationships that
 174 can be derived to express changes in wave angular frequency, power, total
 175 energy flux, and height, due to a tidal current u . Given the wave properties in
 176 the absence of a tidal current (e.g., obtained from a decoupled wave model),
 177 these relationships can be used to compute wave properties in the presence
 178 of a tidal current.

179 *2.2.2. Discussion of limitations of the proposed method*

180 To reliably apply the proposed method to realistic case studies, it is neces-
 181 sary to clearly establish its limitations. Besides the assumptions already dis-
 182 cussed in the above derivations, limitations in the applicability of the method
 183 result from an increase in wave nonlinearity, possibly leading to wave break-
 184 ing, and from wave blocking due to opposing currents. When waves prop-
 185 agate into an opposing currents, their wavelength and group velocity (i.e.,
 186 $u + C_g$) decrease, leading to an increase in wave height and, consequently, to
 187 steeper (and hence more nonlinear) waves; as steepness increases, waves will
 188 approach their breaking limit. Furthermore, if the current velocity is large
 189 enough, the group velocity may approach zero and waves will be “blocked”
 190 by the current [22]. More details are provided below.

191 **a** *Wave breaking by opposing currents*

192 Miche’s law, which gives the breaking limit in deep water as a maximum
 193 steepness kH_b , was generalized by [23] for arbitrary depth as,

$$\frac{kH_b}{\gamma \tanh kh} = 1 \quad (10)$$

194 where H_b is the breaking wave height and γ a constant parameter known as
 195 the “breaking index”. In shallow water ($\tanh kh \approx kh$), this equation reduces
 196 to the standard depth-induced breaking limit: $H_b/h = \gamma$ (with $\gamma \approx 0.7-0.8$),
 197 whereas in deep water ($\tanh kh \approx 1$), it is identical to Miche’s law, with the
 198 recommended value $\gamma \simeq 0.6$ based on experimental data, $kH_b = 0.60$ [22].

199 The increase in wave steepness as a function of an of opposing current
 200 velocity is plotted in Fig. 1, based on the equations in Section 2.2. For

instance, an opposing current with $u/C_o = 0.15$, approximately doubles wave steepness. Hence, for a wave of period 9 s, $C_o = 11.7$ m/s and $u = 1.7$ m/s (about 3 knots); a wave with this period and a steepness $kH \simeq 0.3$ in the absence of currents will break when facing a 3 knot current.

b *Wave blocking by opposing currents*

For sufficiently strong currents, the propagation of wave energy will be stopped, i.e., wave blocking will occur. In deep water, the dispersion equation reads

$$\sigma^2 = (\sigma_o - uk)^2 = gk \Rightarrow \sigma_o - uk = \sqrt{gk}, \quad (11)$$

implying that, for a given absolute frequency σ_o and opposing current velocity u , the solution of this equation is at the intersection between a line (LHS) and a curve (RHS). Fig. 2 shows graphically the solution of the dispersion equation for three different cases, assuming waves are traveling in the x direction ($k > 0$) and facing an opposing currents $u < 0$: no current, an opposing current of less than the stopping velocity, and a current equal to the stopping velocity. If the current (slope of lines) is large enough, the line becomes tangential to the curve; as this is a limiting case, no solution exists for larger velocities. This limiting velocity is referred to as the stopping velocity and corresponds to a zero group velocity, for which waves will be completely blocked by the opposing current. An expression for the stopping velocity can be derived, by specifying the “tangent” condition, $d\sqrt{gk}/dk = -u_s$, in Eq. 11 as [24]

$$u_s = -\frac{g}{4\sigma_o} \quad (12)$$

221 For the above example of a wave with a 9 s period, the stopping velocity
 222 is 3.5 m/s (or 7 knots). Tidal currents of this strength only occur at a few
 223 specific high-energy locations suitable for tidal energy development (e.g. [25])
 224 or in tidal inlets, but rarely exist at wave energy sites. If $|u| < u_s$ for the
 225 opposing current, the dispersion equation has 2 solutions (points A and B in
 226 Fig. 2), the first one (point A) representing a wave with shorter wavelength
 227 than without a current, while the second one (point B) representing very
 228 short length waves, which are reflected by the current; in both cases, wave
 229 energy is transported in the positive x direction. A more detailed discussion
 230 has been provided elsewhere [24] .

231 **c** *Nonlinearity*

232 An opposing current increases wave steepness and thus nonlinearity, mak-
 233 ing waves both skewed and asymmetric (i.e., both front-to-back and trough
 234 to crest); the phase speed of strongly nonlinear waves also depends on wave
 235 height.

236 Spectral operational wave models, such as SWAN, which have been cou-
 237 pled with hydrodynamic models (e.g., ADCIRC or ROMS [26, 27]) do not
 238 simulate such nonlinear effects and are based on linear wave theory [28]. Fully
 239 nonlinear wave-current interaction models have been developed in the time
 240 domain, but are computationally expensive and prohibitive for performing
 241 the long-term simulations required for wave energy resource assessments (e.g.,
 242 [28]). Using a very similar formulation to that discussed in Section 2.1, and
 243 based on a comparison of the linear and nonlinear dispersion relationships
 244 with experimental data, Chawla and Kirby [22] showed that nonlinearity is

only important close to the breaking or blocking points. This is confirmed in Fig. 3, which compares the linear and (3rd-order [22]) nonlinear dispersion relationships, in deep water for $H = 2$ m, and shows that the linear equation is accurate up to $\sigma \simeq 1.2$ r/s, corresponding to $kH \simeq 0.3$; for larger steepnesses, discrepancies with the nonlinear equation gradually increase up to the breaking point. The third-order dispersion relationships for periodic Stokes waves in arbitrary depth is given by

$$\sigma = \sqrt{gk \tanh kh \left[1 + \left(k \frac{H}{2} \right)^2 \left(\frac{8 + \cosh 4kh - 2 \tanh^2 kh}{8 \sinh^4 kh} \right) \right]} \quad (13)$$

which is clearly steepness dependent.

In summary, based on the above discussion, the simplified methodology proposed in this paper is only valid for moderate wave steepness $kH \ll 0.6$, perhaps up to $kH = 0.3$, i.e., for waves that are not close to the breaking point. Additionally, the tidal current should be significantly less than the stopping velocity for the considered waves, $u \ll u_s$. These assumptions will be found to be often valid for the realistic sites discussed in the next sections.

3. Field data for validating the proposed method

The simple analytical method presented above is valid for any site where the assumptions made are realistic, i.e., linear deep water waves over a stationary current. As indicated, however, it is also hoped that the method would apply to waves that have already somewhat entered the intermediate water depth regime. This will be verified using field data.

265 In the following, we assess the performance of the simplified method for
 266 two sites on the UK shelf, in which wave data was collected using wave
 267 buoys (Fig. 4) : (i) Pentland Firth, south of Orkney, and (ii) Scarweather,
 268 in the Bristol Channel. Figs. 5a,c show time series of significant wave height
 269 measured at the two sites during 15 days in March 2012 and January 2007,
 270 respectively; we see that these are fairly energetic sites, with H_s varying
 271 between 1-4 and 1-5 m, respectively. The corresponding wave periods vary
 272 between 6 s and 10 s for these time series. Fig. 6 shows typical wave fields, in
 273 the form of average significant wave heights and direction, computed around
 274 the two selected sites using the SWAN wind-wave model, during the periods
 275 of field data collection at the buoys. The SWAN model and its set-up have
 276 been described in [3, 9]. We see that the prevailing wave direction is eastward
 277 around both sites.

278 Representative time series of tidal current velocity were simulated around
 279 the two selected sites using the ROMS model. A detailed description of
 280 tide modeling has been presented elsewhere [25, 9], and Table 3 gives the
 281 ROMS model configuration at the two selected sites. Fig. 7 shows the tidal
 282 ellipses computed at each site based on these simulations; we see that the
 283 dominant current direction is approximately east-west at each site. Hence, it
 284 is reasonable to assume that waves are almost aligned with the tidal currents
 285 at both locations.

286 As a results of the energetic wave conditions and strong tidal currents, in
 287 recent years, the Orkney archipelago has attracted much attention for wave
 288 and tide energy development. The establishment of the European Marine
 289 Energy Center (EMEC) in Orkney was a key step towards the development of

290 wave power harvesting, together with ambitious plans for developing 1.6 GW
 291 of marine renewable energy by 2020, in this region [29]. Although the wave
 292 energy resource of the Bristol Channel is less than that of Orkney [30], some
 293 wave energy devices have been tested in this area. Furthermore, due to the
 294 presence of strong tidal currents, a number of researchers have shown some
 295 interest in studying wave-tide interactions in both regions [10, 31, 32, 33].

296 *3.1. Frequency and time domain analysis*

297 Astronomical tides have predetermined periods, which are controlled by
 298 the relative motion of the Earth-Moon-Sun system. Therefore, waves that
 299 have been strongly affected by tides should show signs of modulations at the
 300 periods associated with astronomical tides. The principal lunar (M2) and
 301 solar (S2) semidiurnal constituents, with periods of 12.42 hr and 12.00 hr,
 302 respectively, are the most important tidal components around the sites of
 303 interest [34]. As an example, Fig. 8a shows an idealized signal, which has
 304 been modulated by tides resulting from M2, S2, and M4 constituents. The
 305 M4 super-harmonic tidal component - with a period of 6.41 hr - has made
 306 the modulation slightly asymmetric [25]. This time series can be decomposed
 307 into two signals as follows,

$$f(t) = f_o(t) + f_{Tide}(t) \quad (14)$$

308 where f_o is the signal in the absence of tides and f_{Tide} results from the tidal
 309 effects. One way to separate and evaluate the tidal effects is to transform
 310 the time series to the frequency domain using a fast Fourier transform (FFT,
 311 [35, 36]). This is done in Fig. 8b, where we see that the magnitude and

312 period of each tidal constituent's effect can be separated using this method.
 313 After transforming the signal to the frequency domain, tidal effects could be
 314 removed by passing the signal through a band-stop or notch filter [36] and
 315 applying an inverse FFT. This procedure will be applied to data measured at
 316 both sites, to identify tidal current effects on wave properties and compare
 317 results with those of the proposed simplified method. Note, this method has
 318 limitations, as it is assumed that the two signals are linearly superimposed
 319 and nonlinear interactions can be ignored.

320 Thus, the procedure was applied to the time series of significant wave
 321 height collected at both field sites (Figs. 5a,c). Figs. 5b,d shows both
 322 signals transformed in the frequency domain, where we clearly see the effect
 323 of the M2 tidal component on the wave height, with a period of 12.42 hr.

324 4. Results

325 In Fig. 9, we computed the ratio of wave properties in the presence and
 326 absence of a tidal current, using the simplified method described in Section
 327 2.2 and summarized in Table 2, for a range of wave periods T and current
 328 velocities u . This figure also demonstrates that using the complete equations
 329 (i.e. Section 2.2) does not lead to a significant difference. Results were
 330 calculated for a nominal 40 m water depth, assuming deep water conditions;
 331 however, using the complete equations, it can be shown, that these are not
 332 very sensitive to the water depth for this range of wave parameters.

333 In Fig. 9, we see that, as expected, wave height increases/decreases for
 334 an opposing/following current, respectively. In the former case, this effect is
 335 magnified for the (relative) wave power, which is proportional to the square

336 of wave height. The amplification is less for the wave energy flux - or the
 337 absolute wave power observed by a stationary observer - since opposing cur-
 338 rents, in general, slow down the transport velocity of wave energy. In Fig. 9a,
 339 the power amplification factor collapses onto a single curve when the current
 340 velocity is normalized by wave celerity; but, in Fig. 9b it varies for different
 341 wave periods, as a function of the current velocity. For instance, $u = -2$ m/s
 342 corresponds to three values of $u/C_0 = 2\pi u/(gT) = 0.14, 0.16$ and 0.18 in
 343 other subplots, corresponding to wave periods of 7, 8 and 9 seconds; there-
 344 fore, three different values of P/P_o also correspond to $u = -2$ m/s. For
 345 co-flowing currents, wave height decreases, while the wave energy propaga-
 346 tion velocity increases (i.e. $C_g + u$). The former has more effect on the wave
 347 energy flux than the latter, which leads it to decrease. For a site with an
 348 opposing current velocity of about 1.5 m/s, wave power increased by up to
 349 100% (or 60% in wave height), and the effect is even more pronounced for
 350 lower energy (shorter period) waves. The increased effect of tides in regions
 351 with lower wave energy has been reported in other research [8, 9].

352 The accuracy of these predictions was first assessed for the Pentland Firth
 353 site. Fig. 10a shows a subset of the time series of significant wave height
 354 measured at this site (Fig. 5). As mentioned before, for irregular waves,
 355 the equations derived for the simplified method assuming monochromatic
 356 waves can be used by replacing H by H_{RMS} , which is proportional to H_s ;
 357 hence, $H/H_o \rightarrow H_{RMS}/H_{o,RMS} = H_s/H_{os}$. Using the observed time series
 358 of H_s values in Fig. 10a, the tidal modulation was filtered out, as detailed
 359 in Section 3.1, and the remaining signal was treated as the significant wave
 360 height in the absence of tides, H_{os} ; the ratio of wave height in the presence

361 and the absence of tides, $H/H_o = H_s/H_{os}$, was then calculated. The time
 362 series of this ratio is plotted in Fig. 10b and compared to that predicted by
 363 the simplified method, based on tidal current velocities estimated from the
 364 tidal ellipses (Fig. 7) computed at the site (Fig. 10c). Considering in Fig. 10
 365 a time period during which the significant wave height was relatively large
 366 (more than 1 m; marked by vertical lines), we see in Fig. 10b that, despite the
 367 many assumptions behind the simplified method, it can accurately capture
 368 both the frequency and magnitude of the tidal modulation.

369 This is confirmed in Fig. 11, which shows a comparison in the frequency
 370 domain of wave height ratios (i.e., $H/H_o = H_s/H_{os}$ observed for irregular
 371 waves; Fig. 10) at the Pentland Firth site to those predicted using the
 372 simplified method, with and without tidal current. In Fig. 10a, we see that
 373 the observed time series of H_s/H_{os} is approximately a harmonic function
 374 of amplitude 0.1, oscillating around 1.0, with a period of about 12.41 hr
 375 (i.e. $y(t) = 1 + 0.1 \sin 2\pi/12.41t$). This is clearer in Fig. 11 where we see,
 376 after performing a Fourier transform, that the simplified method predicts
 377 the period and amplitude of the modulations of the observed wave height
 378 ratio within 2%, confirming its predictive ability near the M2 principal tidal
 379 constituent period, which dominates tidal effects at the selected study sites.
 380 The same analysis was repeated for the Scarweather site. Results are reported
 381 in Figs 12 and 13, which demonstrate a level of accuracy similar to that of
 382 the Pentland Firth site (i.e. less than 2% error for period and amplitude of
 383 the modulation in Fig. 13).

384 5. Discussion

385 Besides the assumptions introduced in Section 2.1, other considerations
386 should be taken into account when applying the simplified method. The effect
387 of tidal elevation variations was ignored, as it was previously shown (using
388 coupled models), that this parameter has much less effect on wave power
389 than currents [9]. Assuming linear wave theory also implies that the actual
390 sea state is approximated by a superposition of harmonic waves, in which
391 no sinks or sources of energy interact with the wave field. This assumption
392 would not lead to a significant error, since the method is only locally applied
393 to a wave field, which has already been generated by proper sources and sinks
394 of energy, and faces a current field.

395 A model such as SWAN can include effects of the ambient current field
396 in the wave simulation. However, special care should be taken to extract
397 and interpret the wave power predicted in these models in the presence of
398 currents. For instance, SWAN’s output variable ‘TRANSP’ (Energy trans-
399 port), which is often used to evaluate the wave power, actually represents
400 the relative wave power (i.e. $\int C_g E d\sigma$ [37]). The wave energy transport, or
401 absolute wave power, is $\int (C_g + u) E d\sigma$ (Eq. 4), which, to the best of the
402 authors’ knowledge, is not available as an output variable.

403 Assessing the wave resource at a specific site involves two steps; charac-
404 terizing, (1) the theoretical wave energy resource, and (2) the technical wave
405 energy resource. The extractable power P_{Tech} (i.e., the technical power) from
406 a wave energy converter is a function of wave height and period at a site (i.e.,
407 theoretical wave energy resource), and of the efficiency of the device. This

408 can be expressed as

$$P_{Tech} = f(H_s, T_e) = C_p(H_s, T_e)E_f(H_s, T_e) \quad (15)$$

409 where f denotes a function (i.e., power matrix), which implicitly includes the
410 efficiency of the device, C_p is the power coefficient, and E_f the theoretical
411 wave power or total wave energy flux at the studied location. To perform
412 theoretical resource assessments, three methods are usually used. The first
413 one estimates wave power using an uncoupled wave model (e.g., SWAN)
414 that ignores tidal effects. For such a case, this paper provides a method by
415 which the effects of tidal modulations can be superimposed on time series of
416 wave height predicted by the uncoupled model. The second method is to use
417 observed data (e.g., collected at a wave buoy), in which the effects of tide
418 on the wave resource are implicitly included. In this case, the methodology
419 presented in this paper can be used to clearly identify the tide-induced modu-
420 lations/contributions in/to the wave power. More importantly, the proposed
421 methods can help generalize such effects to longer time series for which there
422 are no observed data. Rarely, a third method consisting in applying fully
423 coupled wave-tide models may be used for wave resource assessment, and in
424 this case the proposed analytical/simplified methods can provide insight into
425 model results and their interpretations.

426 Finally, note that in terms of technical resource assessment, this research
427 does not investigate the possible effects of wave-tide interactions on power
428 curves, which are device-dependent and hence cannot be generalized to all
429 devices. However, it helps provide better estimates of technical power by per-
430 forming a more accurate assessment of wave height at a site that is influenced

431 by tides (theoretical resource).

432 As mentioned before, opposing and following currents lead to an increase
433 or decrease in wave height, respectively. However, this effect is highly asym-
434 metrical for the wave height and other quantities related to wave energy, for
435 each current direction (Fig. 9). To further analyze the practical implications
436 of this observation, we considered a single Pelamis device, rated at 750 kW,
437 whose power matrix is plotted in Fig. 14, for multiple combinations of signif-
438 icant wave height and period [38]. It can be inferred from this matrix that -
439 for a constant wave period - the modulation of wave height by a tidal current
440 can lead to significant variations in wave power output of the device, while
441 for a constant wave height, the wave power is less sensitive to a small varia-
442 tions in the wave period. Fig. 15 shows an idealized case for which overall
443 effects of tidal currents on the technical wave power that can be extracted
444 from a device has been examined. For simplicity a constant wave period of 9
445 s was considered in Fig. 15a. It is clear from Fig. 15c that the overall effects
446 of the current is an increase of wave energy. For this case, the integral of the
447 wave power time series over a 15 day period is 89.9 MWh and 95.2 MWh in
448 the absence and presence of a tidal current, respectively. One should cau-
449 tion, however, while tidal currents can increase the extractable wave power,
450 they may lead to difficulties in the operation of wave energy devices, and
451 consequently reduced efficiency.

452 6. Conclusions

453 We presented a simplified method, based on linear wave theory, which can
454 be used to predict the effects of tidal currents on the wave power resource.

455 The method demonstrates that one can expect a significant increase in wave
456 height and power when currents are opposing waves (e.g., a 60% increase in
457 wave height for a -2.0 m/s current and a 8 s wave period), and a decrease in
458 these quantities, albeit smaller, when waves are following the currents (e.g.,
459 a 20% decrease in wave height for a +2.0 m/s current and a 8 s wave period).
460 Because of this asymmetrical effect of a current on wave properties, the net
461 effect of a symmetrical tidal current is an increase of the wave energy at a
462 given location; hence, in this case, the overall extractable wave energy by a
463 device also increases.

464 The accuracy of the simplified method was shown to be adequate for
465 two field sites of interest, by comparing results with observed data. It was
466 assumed that waves and currents are approximately aligned with each other,
467 which is valid in the selected wave energy sites, and others, and in most
468 laboratory studies of wave-current interaction.

469 At a wave energy site where currents are significant, energy transfer com-
470 ponents such as the kinetic energy of currents, energy exchange between cur-
471 rents and waves, relative wave power, and total wave energy transfer should
472 be carefully considered to realistically assess the technically extractable wave
473 energy resource. It should be noted that the presence of tidal currents may
474 reduce the performance of a tidal energy converter if it was designed assuming
475 no flow conditions.

476 7. Acknowledgements

477 Thanks to Cefas WaveNet for supplying the wave buoy data at Scar-
478 weather, and to Philippe Gleizon (University of the Highlands and Islands,

479 Thurso) for providing wave buoy data at Pentland Firth. S.P. Neill ac-
480 knowledges financial support provided by the Welsh Government and Higher
481 Education Funding Council for Wales through Sêr Cymru National Research
482 Network for Low Carbon Energy and the Environment

483 References

- 484 [1] M. E. McCormick, Ocean wave energy conversion, Courier Corporation,
485 2013.
- 486 [2] F. d. O. Antonio, Wave energy utilization: A review of the technologies,
487 Renewable and sustainable energy reviews 14 (2010) 899–918.
- 488 [3] S. P. Neill, M. J. Lewis, M. R. Hashemi, E. Slater, J. Lawrence, S. A.
489 Spall, Inter-annual and inter-seasonal variability of the orkney wave
490 power resource, Applied Energy 132 (2014) 339–348.
- 491 [4] ABPmer, Atlas of UK marine renewable energy resources, Technical Re-
492 port, Department for Business Enterprise & Regulatory Reform, 2008.
- 493 [5] R. Soulsby, L. Hamm, G. Klopman, D. Myrhaug, R. Simons, G. Thomas,
494 Wave-current interaction within and outside the bottom boundary layer,
495 Coastal engineering 21 (1993) 41–69.
- 496 [6] N. Guillou, G. Chapalain, Modeling the tide-induced modulation of
497 wave height in the outer seine estuary, Journal of Coastal Research 28
498 (2012) 613–623.
- 499 [7] J. M. Brown, A. G. Davies, Methods for medium-term prediction of
500 the net sediment transport by waves and currents in complex coastal
501 regions, Continental Shelf Research 29 (2009) 1502–1514.
- 502 [8] F. Barbariol, A. Benetazzo, S. Carniel, M. Sclavo, Improving the as-
503 sessment of wave energy resources by means of coupled wave-ocean nu-
504 merical modeling, Renewable Energy 60 (2013) 462–471.

- 505 [9] M. R. Hashemi, S. P. Neill, The role of tides in shelf-scale simulations
506 of the wave energy resource, *Renewable Energy* 69 (2014) 300–310.
- 507 [10] A. Saruwatari, D. M. Ingram, L. Cradden, Wave–current interaction
508 effects on marine energy converters, *Ocean Engineering* 73 (2013) 106–
509 118.
- 510 [11] F. Maerins, P. Leitão, A. Silva, R. Neves, 3D modelling in the Sado es-
511 tuary using a new generic vertical discretization approach, *Oceanologica*
512 *Acta* 24 (2001) 51–62.
- 513 [12] N. Barltrop, K. Varyani, A. Grant, D. Clelland, X. Pham, Wave-current
514 interactions in marine current turbines, *Proceedings of the Institution of*
515 *Mechanical Engineers, Part M: Journal of Engineering for the Maritime*
516 *Environment* 220 (2006) 195–203.
- 517 [13] M. Lewis, S. Neill, M. Hashemi, Realistic wave conditions and their in-
518 fluence on quantifying the tidal stream energy resource, *Applied Energy*
519 136 (2014) 495–508.
- 520 [14] R. A. Dalrymple, R. G. Dean, *Water wave mechanics for engineers and*
521 *scientists*, Prentice-Hall, 1991.
- 522 [15] M. S. Longuet-Higgins, R. Stewart, Changes in the form of short gravity
523 waves on long waves and tidal currents, *Journal of Fluid Mechanics* 8
524 (1960) 565–583.
- 525 [16] G. B. Whitham, *Linear and nonlinear waves*, volume 42, John Wiley &
526 Sons, 2011.

- 527 [17] N. Booij, R. Ris, L. H. Holthuijsen, A third-generation wave model
528 for coastal regions: 1. Model description and validation, *Journal of*
529 *Geophysical Research: Oceans* 104 (1999) 7649–7666.
- 530 [18] G. Whitham, A general approach to linear and non-linear dispersive
531 waves using a lagrangian, *Journal of Fluid Mechanics* 22 (1965) 273–
532 283.
- 533 [19] F. P. Bretherton, C. J. Garrett, Wavetrains in inhomogeneous moving
534 media, *Proceedings of the Royal Society of London. Series A. Mathe-*
535 *matical and Physical Sciences* 302 (1968) 529–554.
- 536 [20] L. H. Holthuijsen, *Waves in oceanic and coastal waters*, Cambridge Uni-
537 *versity Press*, 2007.
- 538 [21] B. Drew, A. Plummer, M. N. Sahinkaya, A review of wave energy
539 converter technology, *Proceedings of the Institution of Mechanical En-*
540 *gineers, Part A: Journal of Power and Energy* 223 (2009) 887–902.
- 541 [22] A. Chawla, J. T. Kirby, Monochromatic and random wave breaking at
542 blocking points, *Journal of Geophysical Research: Oceans* 107 (2002).
- 543 [23] J.-F. Filipot, F. Ardhuin, A. V. Babanin, A unified deep-to-shallow wa-
544 ter wave-breaking probability parameterization, *Journal of Geophysical*
545 *Research: Oceans* 115 (2010).
- 546 [24] R. Moreira, D. Peregrine, Nonlinear interactions between deep-water
547 waves and currents, *Journal of Fluid Mechanics* 691 (2012) 1–25.

- 548 [25] S. P. Neill, M. R. Hashemi, M. J. Lewis, The role of tidal asymmetry in
549 characterizing the tidal energy resource of Orkney, *Renewable Energy*
550 68 (2014) 337–350.
- 551 [26] J. C. Dietrich, J. Westerink, A. Kennedy, J. Smith, R. Jensen, M. Zil-
552 jlema, L. Holthuijsen, C. Dawson, R. Luettich Jr, M. Powell, et al.,
553 Hurricane gustav (2008) waves and storm surge: hindcast, synoptic anal-
554 ysis, and validation in southern louisiana, *Monthly Weather Review* 139
555 (2011) 2488–2522.
- 556 [27] J. C. Warner, B. Armstrong, R. He, J. B. Zambon, Development of a
557 coupled ocean–atmosphere–wave–sediment transport (coawst) modeling
558 system, *Ocean modelling* 35 (2010) 230–244.
- 559 [28] S. Ryu, M. Kim, P. J. Lynett, Fully nonlinear wave-current interactions
560 and kinematics by a bem-based numerical wave tank, *Computational*
561 *mechanics* 32 (2003) 336–346.
- 562 [29] G. Allan, P. Lecca, P. McGregor, J. Swales, The economic impacts of
563 marine energy developments: A case study from scotland, *Marine Policy*
564 43 (2014) 122–131.
- 565 [30] S. P. Neill, M. R. Hashemi, Wave power variability over the northwest
566 European shelf seas, *Applied Energy* 106 (2013) 31–46.
- 567 [31] J. Wolf, D. Prandle, Some observations of wave–current interaction,
568 *Coastal Engineering* 37 (1999) 471–485.
- 569 [32] J. Wolf, Coastal flooding: impacts of coupled wave–surge–tide models,
570 *Natural Hazards* 49 (2009) 241–260.

- 571 [33] B. Jones, A numerical study of wave refraction in shallow tidal waters,
572 Estuarine, Coastal and Shelf Science 51 (2000) 331–347.
- 573 [34] M. Hashemi, S. Neill, A. Davies, A numerical study of wave and cur-
574 rent fields around Ramsey island - tidal energy resource assessment,
575 in: XIXth TELEMAC-MASCARET User Conference, Oxford, United
576 Kingdom.
- 577 [35] C. Van Loan, Computational frameworks for the fast Fourier transform,
578 volume 10, Siam, 1992.
- 579 [36] T. P. Krauss, L. Shure, J. N. Little, Signal processing toolbox for use
580 with matlab (1994).
- 581 [37] N. Booij, I. Haagsma, L. Holthuijsen, A. Kieftenburg, R. Ris, A. Van
582 Der Westhuysen, M. Zijlema, Swan cycle iii version 40.41 user manual,
583 Delft University of Technology 115 (2004).
- 584 [38] E. B. Mackay, A. S. Bahaj, P. G. Challenor, Uncertainty in wave energy
585 resource assessment. part 2: variability and predictability, Renewable
586 energy 35 (2010) 1809–1819.
- 587 [39] D. Mollison, Wave climate and the wave power resource, in: Hydrody-
588 namics of Ocean Wave-Energy Utilization, Springer, 1986, pp. 133–156.
- 589 [40] K. Gunn, C. Stock-Williams, Quantifying the global wave power re-
590 source, Renewable Energy 44 (2012) 296–304.

Table 1: List of symbols

List of symbols	
Symbol	Description
C	wave celerity or phase speed
C_g	wave group velocity
E	period-averaged wave energy: $E = \frac{1}{8}\rho g H^2$
E_f	period-averaged wave energy flux: transport of wave energy by group and current velocity: $E = C_g E + u E$
h	water depth
H, H_o	wave height in the presence and absence of a current, respectively [‡]
H_{RMS}, H_s	RMS and significant wave height
H_b	wave height at the breaking point
k	wave number
N	wave action: $N = E/\sigma$
p_D	dynamic pressure resulting from a linear wave
P	relative wave power: transport of wave energy by group velocity $P = C_g E$
P_{Tech}	Technical wave power
T	wave period
T_e	energy wave period, $2\pi m_{-1}/m_0$, where m shows the moment of the wave spectrum [39].
T_{M2}, T_{S2}, T_{M4}	period of M_2 , S_2 , and M_4 astronomical tide components: 12.42 hr, 12.00 hr, and 6.21 hr.
u	tidal current velocity
u_s	stopping velocity
u_w	horizontal wave induced velocity
\mathbf{u}_w	wave induced velocity vector
η	water surface elevation
ρ	water density
σ	intrinsic or relative wave frequency
σ_o	absolute wave frequency: $\sigma_o = \sigma + k u$
γ	breaking index

[‡] the o subscript for all wave properties means these are in the absence of a current (e.g. k_o, σ_o).

Table 2: Change of wave properties as a result of a tidal current u , assuming deep water waves ($kh > \pi$)

Wave property	Equation
wave frequency	$\frac{\sigma}{\sigma_o} = 2 \left[1 + \sqrt{1 + \frac{4u}{C_o}} \right]^{-1} ; C_o = \frac{g}{\sigma_o}$
(relative) wave power	$\frac{P}{P_o} = \frac{E}{E_o} \frac{C_g}{C_{go}} = \frac{\sigma}{\sigma_o} \left[\frac{1}{1 + \frac{2u}{C_o} \frac{\sigma}{\sigma_o}} \right]$
total wave energy flux	$\frac{E_f}{E_{fo}} = \frac{(C_g + u)E}{C_{go}E_o} = \frac{\sigma}{\sigma_o}$
wave height	$\frac{H}{H_o} = \frac{\sigma}{\sigma_o} \left[\frac{1}{1 + \frac{2u}{C_o} \frac{\sigma}{\sigma_o}} \right]^{\frac{1}{2}}$

Table 3: ROMS model set-up used for simulating time series of tidal currents at two sites (Fig. 4).

ROMS Setting	Region	
	Pentland Firth	Bristol Channel
Horizontal resolution	500 m	5000 m
Number of vertical layers	10	11
Bathymetry	GEBCO (www.gebco.net) and data provided by St. Andrew's University	ETOPO (www.ngdc.noaa.gov)
Tidal forcing at the boundaries	FES2012 (www.aviso.altimetry.fr)	TPXO7 (volkov.oce.orst.edu/tides/)
Tidal constituents	M2 and S2	M2, S2 and 8 other component
Drag coefficient	0.003	0.0025
Turbulence model	k- ϵ	k- ϵ
Validation points	Tidal stations around Orkney from the Admiralty tide tables	Tidal stations in the Bristol Channel from the Admiralty tide tables
Accuracy	8 cm for M2 and 4 cm for S2	13 cm for M2 and 7 cm for S2

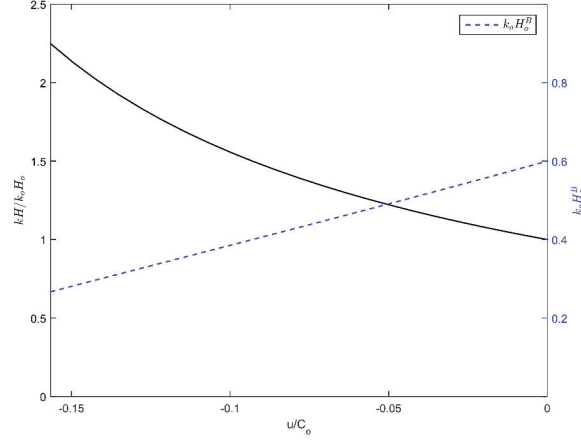


Figure 1: Effect of an opposing current velocity on periodic wave steepness and steepness-induced breaking. The solid curve shows the increase in steepness as a function of current velocity (left axis), and the dashed line shows the threshold for wave breaking (right axis; based on the value of wave steepness without a current).

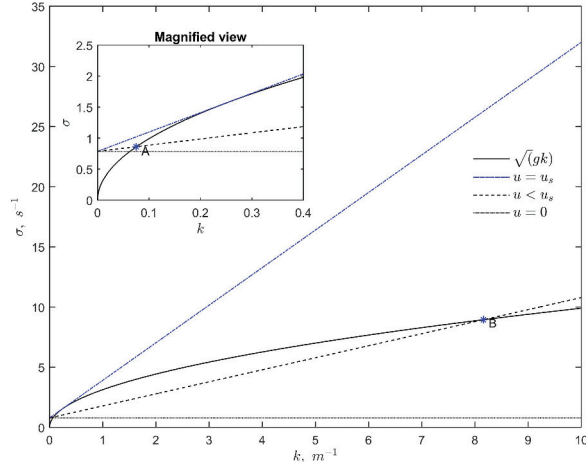


Figure 2: Graphical solution of the linear dispersion relationship, assuming no current (dotted line), an opposing current of less than the stopping velocity u_s (dash line), and a current velocity equal to the stopping velocity (dash-dot line). The solution is at the intersections of the line (i.e., $\sigma_o - uk$) and the curve (i.e., \sqrt{gk}) (e.g., points A and B).

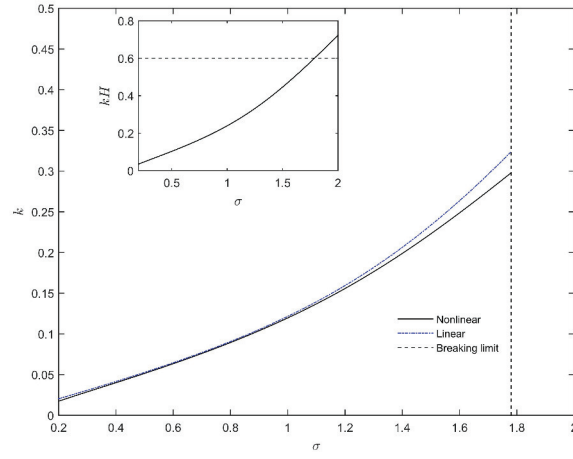


Figure 3: Nonlinear (3rd-order) and linear dispersion relationships for Stokes waves of $H = 2$ m in deep water.

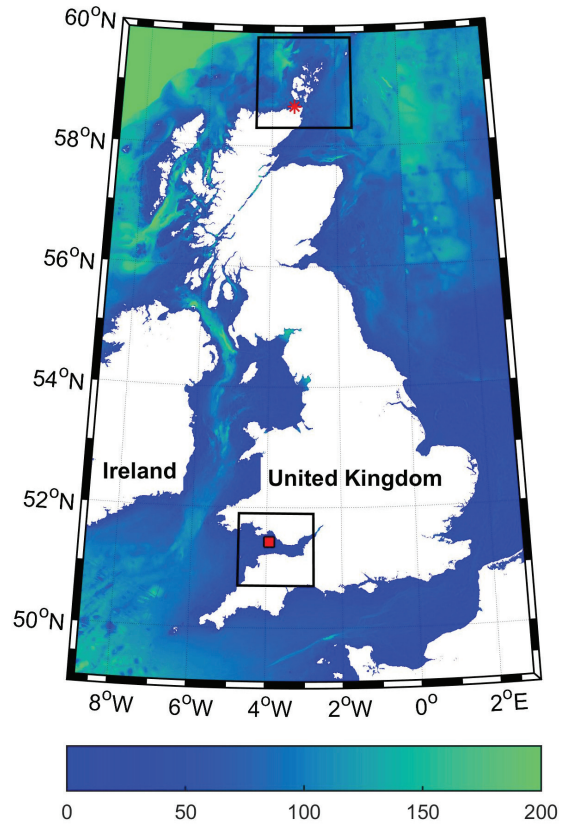


Figure 4: Locations of selected wave buoys for evaluation of wave resource assessment using the simplified method based on field data. The Pentland Firth and Scarweather measurement locations are marked by * and \square symbols, respectively. The average wave climates around these locations - for the period of the analysis - are plotted in Fig. 6, where the rectangles show the extent of the magnified views. Colour scale is bathymetry in meters.

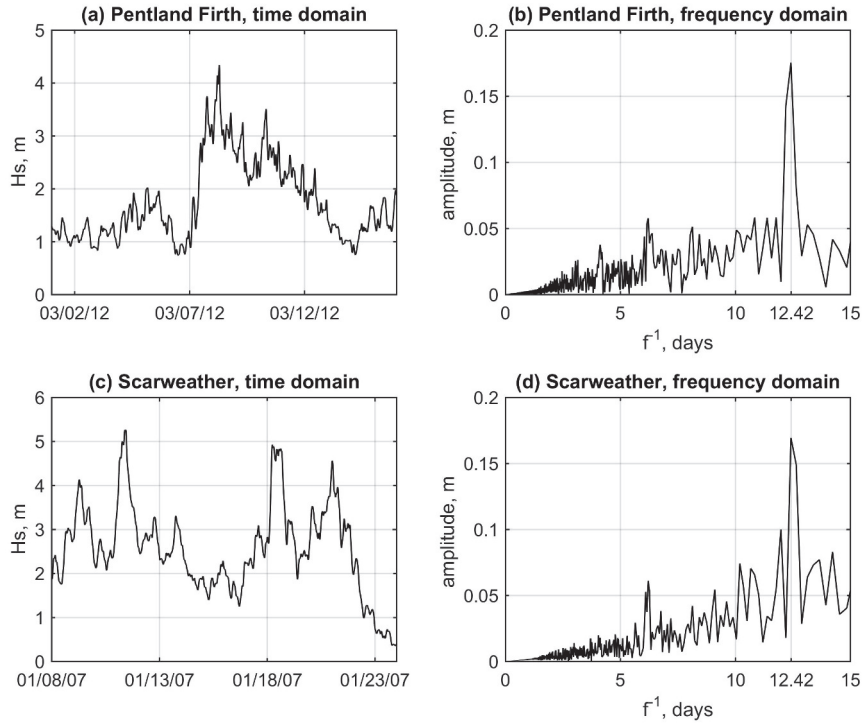
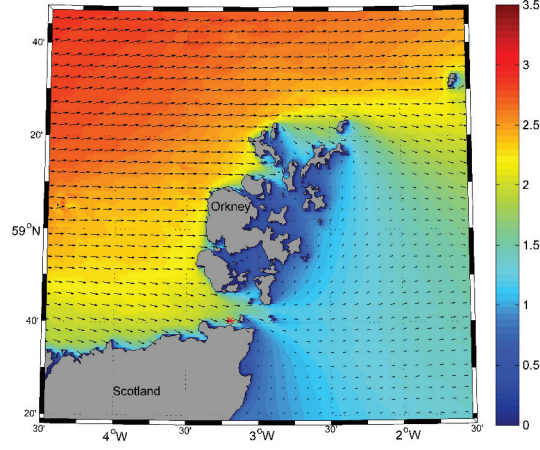
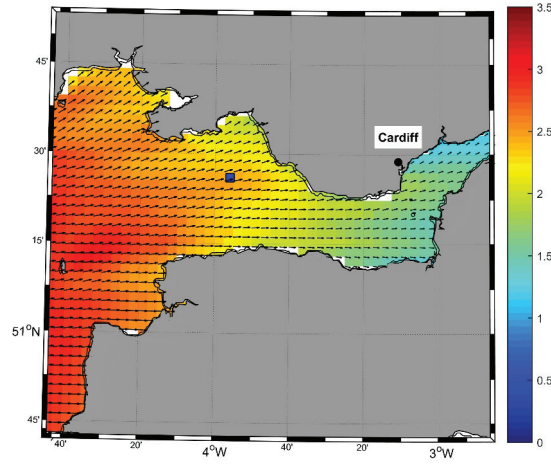


Figure 5: Time series of significant wave height, H_s measured at the Pentland Firth and Scarweather sites (Fig. 4) in March 2012 and January 2007, respectively, during 15 days, which covers a spring-neap cycle (panels a and c). Panels b and d show Fourier transforms of the wave height time series; a clear semidiurnal tidal effect can be observed in the signal at both sites, with the period of the M2 tidal constituent.



(a) Pentland Firth



(b) Scarweather

Figure 6: Mean wave directions around the locations of interest, Pentland Firth and Scarweather sites (Fig. 4), in March 2012 and January 2007, respectively, corresponding to the availability of wave data. The dominant wave directions for these sites follow a very similar pattern in energetic months (i.e., December, January, February and March [30, 3]). The color scales show the average significant wave height H_s in meter for these time periods.

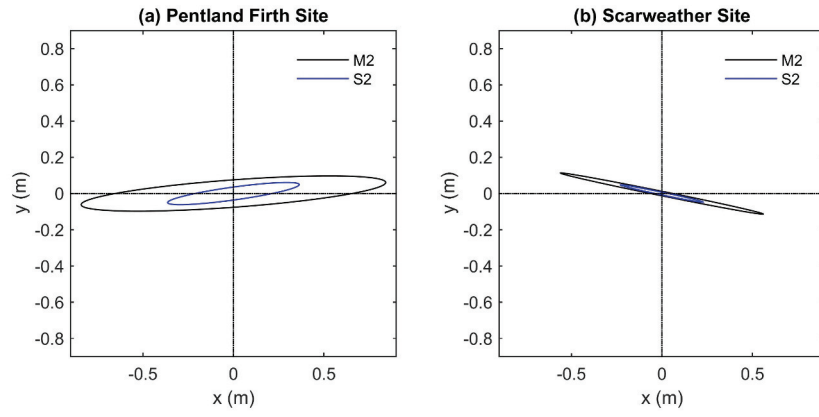


Figure 7: Tidal ellipses for Pentland Firth and Scarweather sites. The tidal currents are generally aligned east-west for both sites.

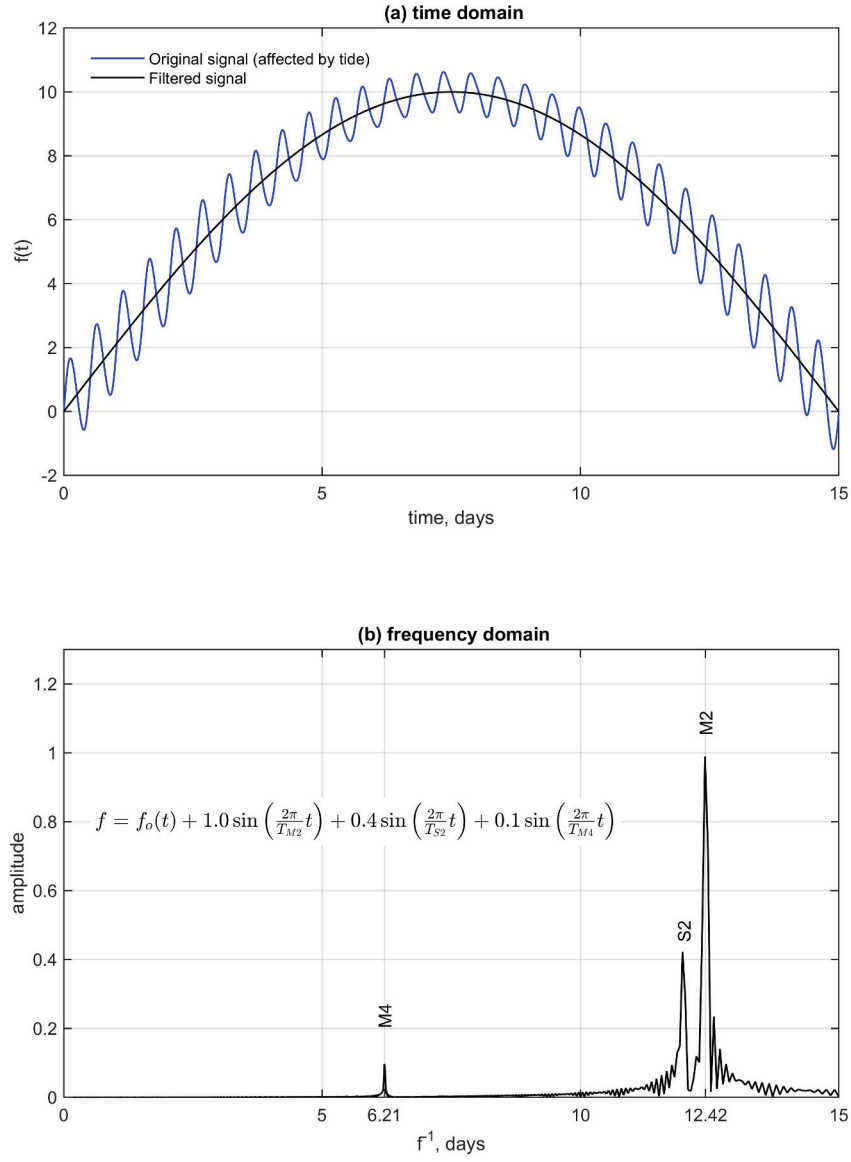


Figure 8: Typical time series with modulation caused by M2, S2, and M4 components: (a) in the time domain, and (b) in the frequency domain.

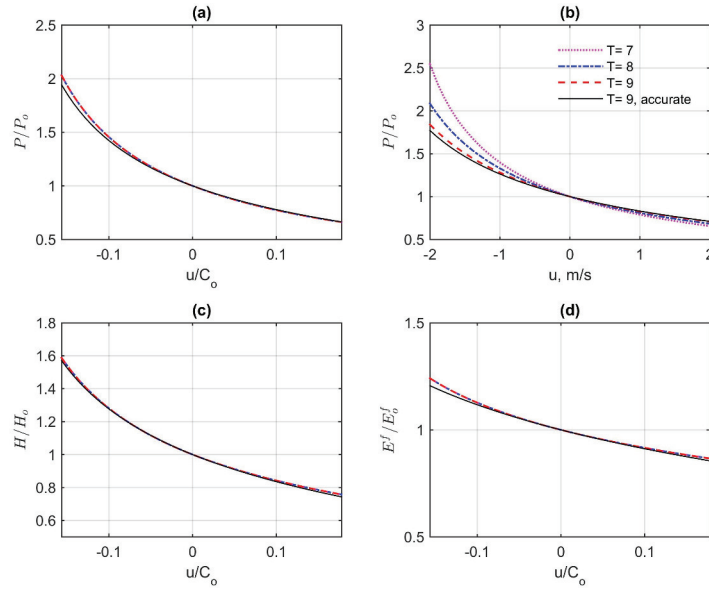


Figure 9: Effects of tidal currents on wave height and power for various wave periods. These linearized results are valid for $kH \ll 0.6$ (see Fig. 1) and $u \ll u_s$ (Eq. 12); subplots a and b show the effect on (relative) wave power, subplot c wave height, and subplot d wave energy flux. The wave properties - in the presence of tidal currents - have been normalized with the corresponding wave-only case. The accurate solutions (for $T = 9$) have been evaluated using the complete equations described in Section 2.2.

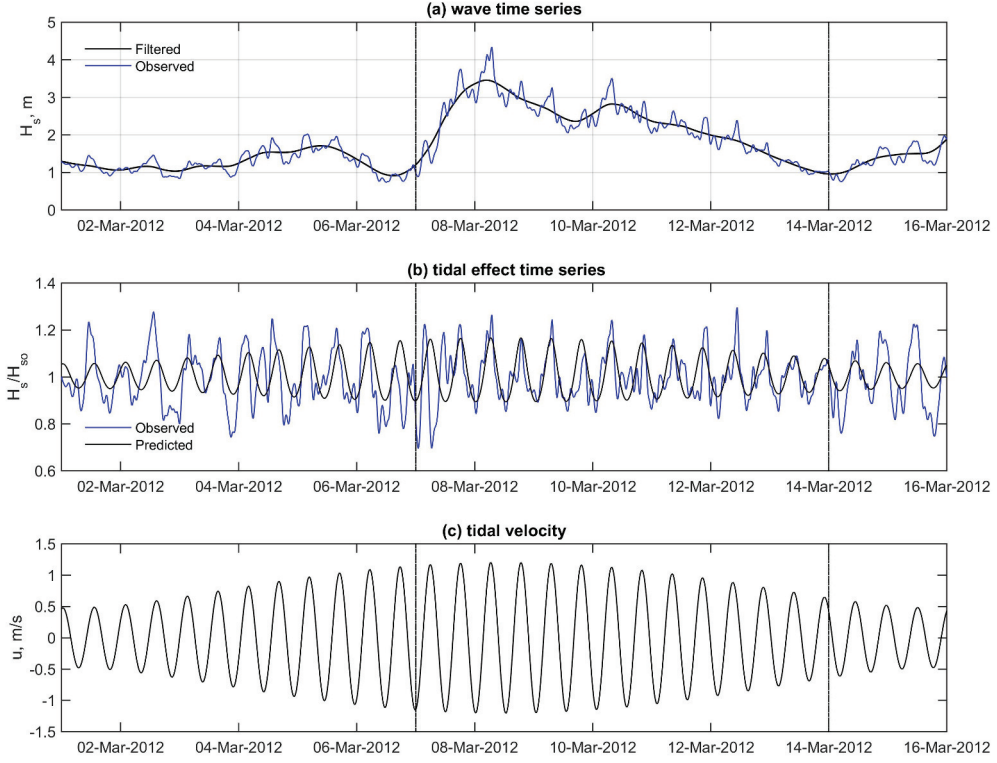


Figure 10: Estimation of tidal current effects using the simplified method for a time series of significant wave height observed at the Pentland Firth site (Fig. 4) during a spring-neap cycle. The tide-induced wave height modulations were filtered out from the signal (panel a), and the resulting wave height ratio compared with the predicted values (panel b; H_s/H_0 is the ratio of wave heights in the presence and absence of a tidal current computed from the two curves in panel a). The tidal current velocity estimated with ROMS is plotted in panel c. The vertical lines mark a time interval during which wave height was relatively large ($H_s > 1$ m), and in panel b the simplified method (predicted curve) provides a good prediction of the tidal-induced modulations, both in magnitude and frequency.

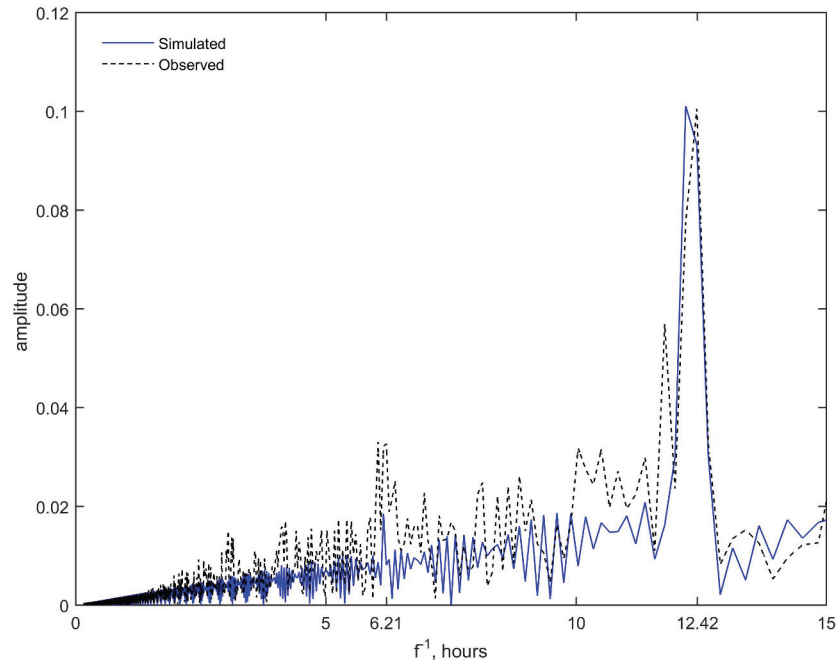


Figure 11: Observed and predicted (using the simplified method) tide-induced wave height ratios, H_s/H_{so} , in the frequency domain, at the Pentland Firth site (Fig. 4). An excellent agreement is observed near the principal tidal constituent's period (i.e., M2 at 12.42 hr).

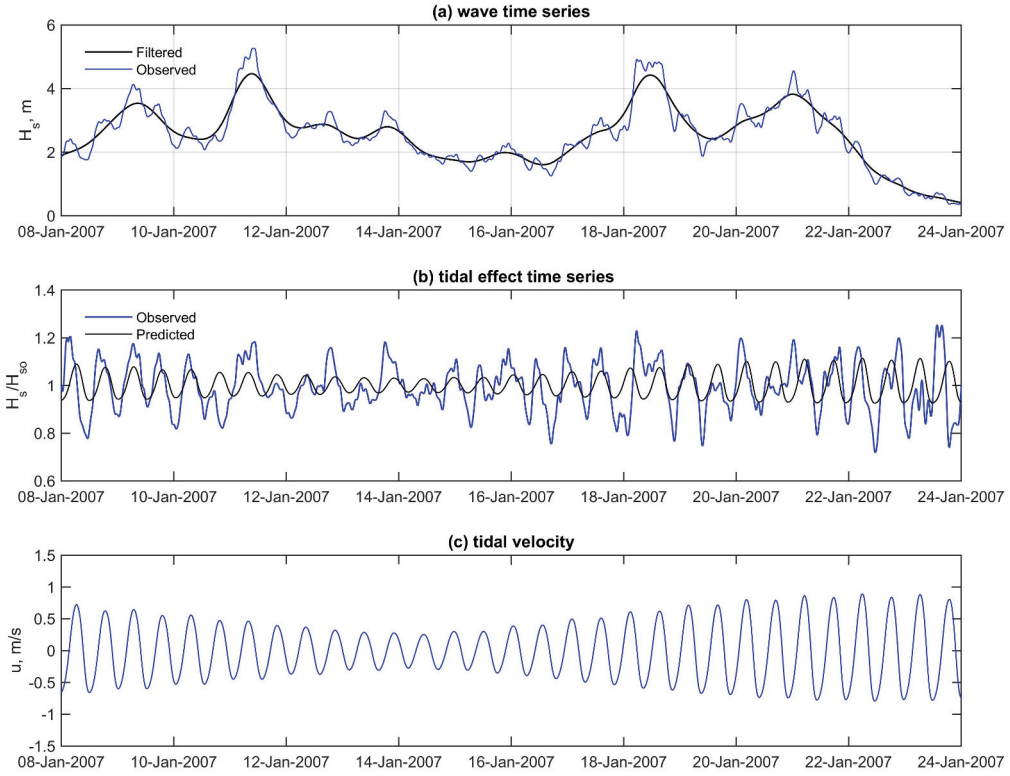


Figure 12: Application of the simplified method of estimating tidal current effects on waves to a time series of significant wave height observed at the Scarweather site (Fig. 4) during a spring-neap cycle. The tide-induced wave height modulations were filtered out from the signal (panel a), and the resulting wave height ratio compared with the predicted values (panel b; H/H_o is the ratio of wave heights in the presence and absence of a tidal current computed from the two curves in panel a). The tidal current velocity estimated with ROMS is plotted in panel c.

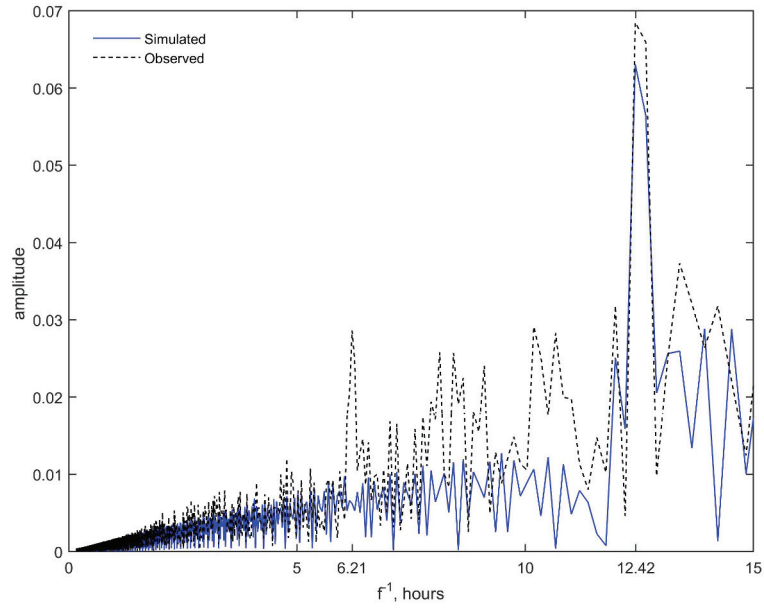


Figure 13: Observed and predicted (using the simplified method) tide-induced wave height ratios, H_s/H_{so} , in the frequency domain, at the Scarweather site (Fig. 4). An excellent agreement is observed near the principal tidal constituent's period (i.e., M2 at 12.42 hr).

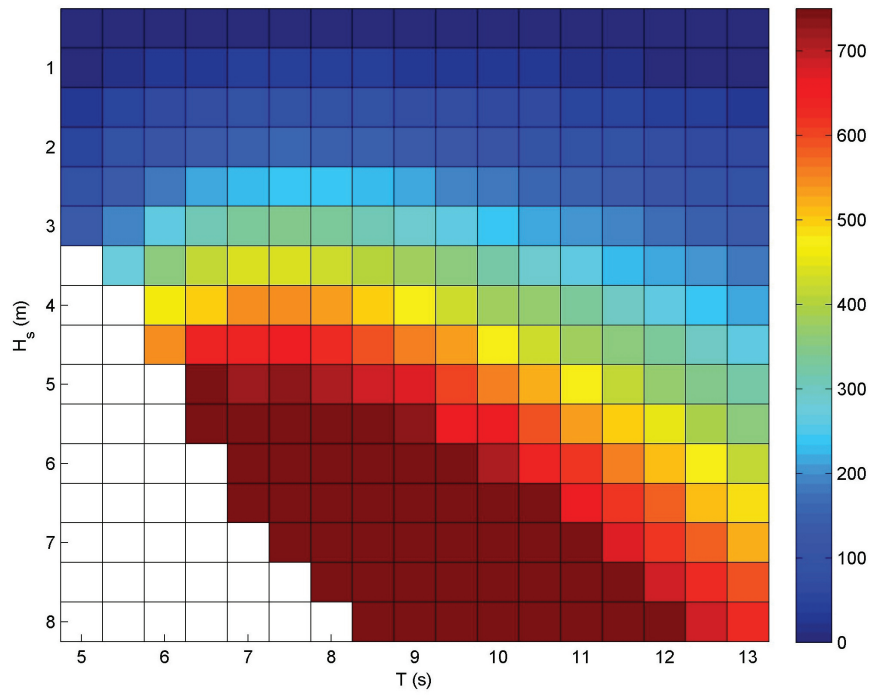


Figure 14: Power matrix of a Pelamis P2 [40] device rated at 750 kW as a function of significant wave height and period. The color scale is Power in kW.

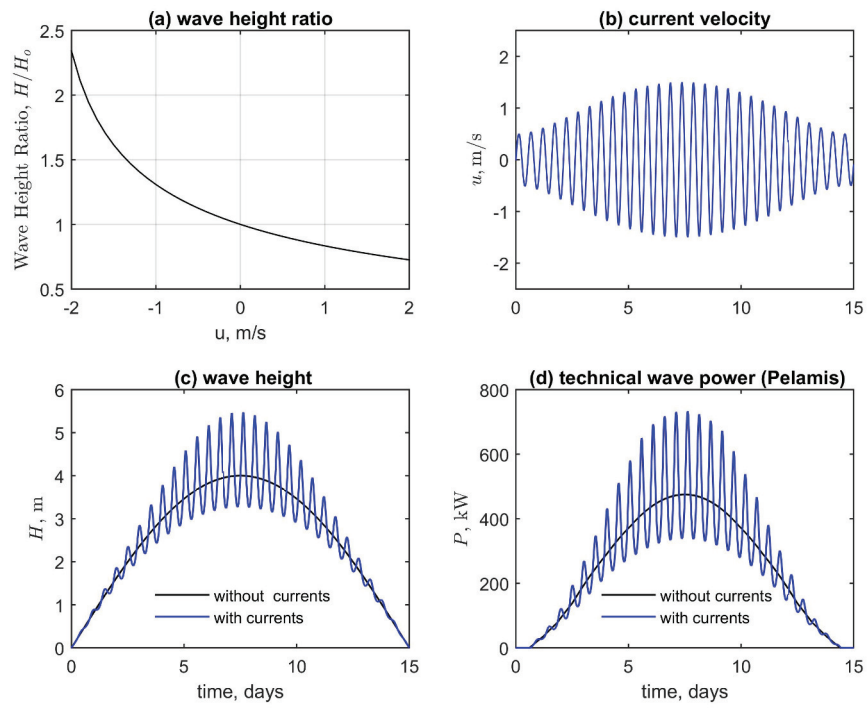


Figure 15: Asymmetric effects of tidal currents on the technical wave power for an idealized wave scenario. For a symmetric tidal current case (panel b), the overall effect is an increase in wave energy, from 89.9 MWh to 95.2 MWh, for the generated wave power depicted in panel d.